# NAVAL POSTGRADUATE SCHOOL
## Monterey, California

AD-A283 524

THESIS

SIMULATIONS OF AN FEL PRODUCING
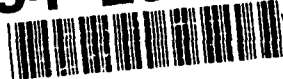COHERENT X RAYS UTILIZING
THE SLAC LINAC

by

Joseph Barry Hall

June 1994

Thesis Advisor:                    William B. Colson

Approved for public release; distribution is unlimited

94-26776

94 8 22 1 2 3

# REPORT DOCUMENTATION PAGE

Form Approved OMB No 0704-0188

| 1. AGENCY USE ONLY *(Leave blank)* | 2. REPORT DATE JUNE 1994 | 3. REPORT TYPE AND DATES COVERED Master's Thesis |
|---|---|---|

| 4. TITLE AND SUBTITLE | 5. FUNDING NUMBERS |
|---|---|
| SIMULATIONS OF AN FEL PRODUCING COHERENT X RAYS UTILIZING THE SLAC LINAC | |

**6. AUTHOR(S)**
Hall, Joseph B.

| 7. PERFORMING ORGANIZATION NAME(S) AND ADDRESS(ES) Naval Postgraduate School Monterey CA 93943-5000 | 8. PERFORMING ORGANIZATION REPORT NUMBER |
|---|---|

| 9. SPONSORING/MONITORING AGENCY NAME(S) AND ADDRESS(ES) Naval Postgraduate School Monterey CA 93943-5000 | 10. SPONSORING/MONITORING AGENCY REPORT NUMBER |
|---|---|

11. SUPPLEMENTARY NOTES The views expressed in this thesis are those of the author and do not reflect the official policy or position of the Department of Defense or the U.S. Government.

| 12a. DISTRIBUTION/AVAILABILITY STATEMENT Approved for public release; distribution is unlimited. | 12b. DISTRIBUTION CODE A |
|---|---|

13. ABSTRACT *(maximum 200 words)*

Due to its tunability and high efficiency, the Free Electron Laser (FEL) has proven to be a versatile coherent light source for a variety of applications in science, industry and defense. This unique capability provides the scientific community with its first realistic source for an X ray laser.

This thesis will initially consider the basics of the FEL and its applications as a defensive weapon. In a technological era where the missile has maximized its physical capabilities to the point that defensive missiles are physically incapable of achieving a kill in protection of the fleet, speed of light weapons are the next logical step in defense. Next we shall explore the theory behind the Free Electron Laser and the amplification of a beam of light by transferring energy from an electron beam.

In conclusion, we examine the proposal to utilize the Stanford Linear Accelerator Center (SLAC) linac as an electron beam source for a high power X ray FEL [1]. Compressing the electron pulse to a sub-picosecond length yields a peak current of 2500 amps. An electron beam energy of 7 GeV would result in a radiation wavelength of 4 nm and peak optical power in the gigawatt range.

In order to examine this proposal, single-mode phase space simulations are run to look at the effectiveness of electron bunching and the onset of saturation. Longitudinal multimode simulations show coherence development and the trapped-particle instability. Transverse multimode simulations examine the effects of optical guiding and mode distortion.

| 14. SUBJECT TERMS X ray FEL; Free Electron Laser; pendulum equation; longitudinal modes | 15. NUMBER OF PAGES 46 |
|---|---|
| | 16. PRICE CODE |

| 17. SECURITY CLASSIFICATION OF REPORT Unclassified | 18. SECURITY CLASSIFICATION OF THIS PAGE Unclassified | 19. SECURITY CLASSIFICATION OF ABSTRACT Unclassified | 20. LIMITATION OF ABSTRACT UL |
|---|---|---|---|

# SIMULATIONS OF AN FEL PRODUCING COHERENT X RAYS UTILIZING THE SLAC LINAC

by

Joseph B. Hall
Commander, United States Navy
A.B., University of Michigan, 1975

Submitted in partial fulfillment
of the requirements for the degree of

## MASTER OF SCIENCE IN PHYSICS
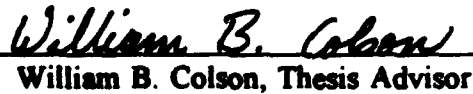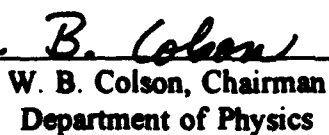
from the

## NAVAL POSTGRADUATE SCHOOL

June 1994

Author: _____
Joseph B. Hall

Approved by: _____
William B. Colson, Thesis Advisor

_____
Robert L. Armstead, Second Reader

_____
W. B. Colson, Chairman
Department of Physics

ii

# ABSTRACT

Due to its tunability and high efficiency, the Free Electron Laser (FEL) has proven to be a versatile coherent light source for a variety of applications in science, industry and defense. This ... ie ...apability provides the scientific community with its first realistic source for a... X .ay laser.

This thesis will initially consider the basics of the FEL and its applications as a defensive weapon. In a technological era where the missile has maximized its physical capabilities to the point that defensive missiles are physically incapable of achieving a kill in protection of the fleet, speed of light weapons are the next logical step in defense. Next we shall explore the theory behind the Free Electron Laser and the amplification of a beam of light by transferring energy from an electron beam.

In conclusion, we examine the proposal to utilize the Stanford Linear Accelerator Center (SLAC) linac as an electron beam source for a high power X ray FEL [1]. Compressing the electron pulse to a sub-picosecond length yields a peak current of 2500 amps. An electron beam energy of 7 GeV would result in a radiation wavelength of 4 nm and peak optical power in the gigawatt range.

In order to examine this proposal, single-mode phase space simulations are run to look at the effectiveness of electron bunching and the onset of saturation. Longitudinal multimode simulations show coherence development and the trapped-

particle instability. Transverse multimode simulations examine the effects of optical guiding and mode distortion.

# TABLE OF CONTENTS

# I. INTRODUCTION

The free electron laser (FEL) consists of a relativistic electron beam which passes through the transverse periodic magnetic field of an undulator. This results in the exchange of energy between the electrons and a copropagating optical wave. Traveling through the undulator the electrons are acted upon by Lorentz forces inducing transverse oscillations. This acceleration causes the electron to emit electromagnetic radiation. The wavelength of this radiation depends on the electron beam energy thereby providing a tunable light source. An FEL configured as an oscillator stores the light in an optical cavity. However, in an FEL configured as an amplifier, light is created and amplified during a single pass of the electrons through the undulator eliminating the need for optics. The FEL has provided high efficiency and power, but its one overriding attribute which enhances its future in science, industry and defense is its ability to provide, on demand, wavelength tunability. As a tunable source of laser light, the FEL is of interest in the infrared and ultraviolet spectrums in the study of solid state physics and molecular spectroscopy. Medicine is another region in which the FEL may play an important role. In the X ray regime, the FEL may lead to holographic imaging of DNA molecules and imaging of live biological microstructures in their normal physiological environments. Finally, the future of the FEL in missile defense may revolutionize naval shipboard defense systems.

## A. DEFICIENCIES OF CURRENT SHIP DEFENSE SYSTEMS

The current systems which comprise the battle group defense in depth has a superior long range capability. However, as the inevitable leaker finds its way into the inner sanctum of the battle group and a single ship is left to defend itself against this highly maneuverable and lethal threat, current capabilities are in need of much improvement. If we examine the system which is the ships final course of defense, the phalanx gun system is the weak link in the chain. Analyzing the phalanx gun through computer simulations, we can first examine a distribution of
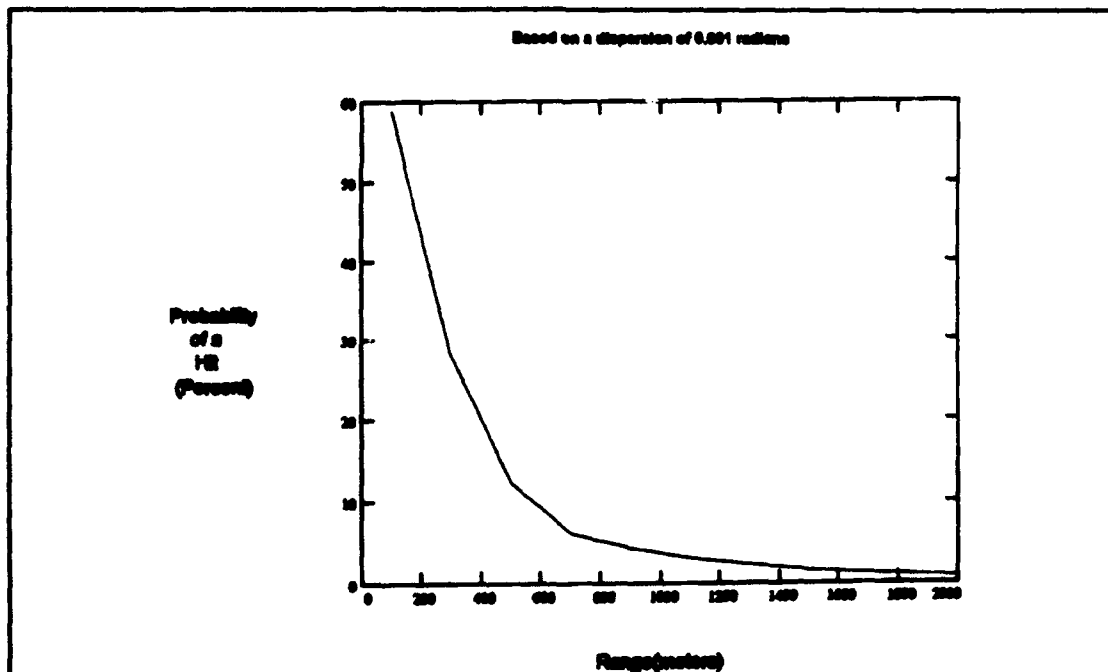


Figure 1-1. Probability of a hit vs. range for a very accurate phalanx gun barrel.

bullets at ranges from 100 meters to 2000 meters using random angular

2

dispersions. Figure 1-1 shows the result for the most accurate barrel system with a dispersion of 0.001 radians. The graph shows an asymptotic decay in the probability of hitting the target as a function of increasing range. From Figure 1-1 we find that we can achieve a maximum probability of a hit of only 60% inside 100 meters against a 25 cm radius target. Further, it is accepted in simulations of the phalanx that 5 hits are required to kill an inbound missile. Therefore, the probability of a kill becomes 8%. Figure 1-2 is another simulation which is based on a missile kill whose debris is then tracked to impact. We find that a kill at 800
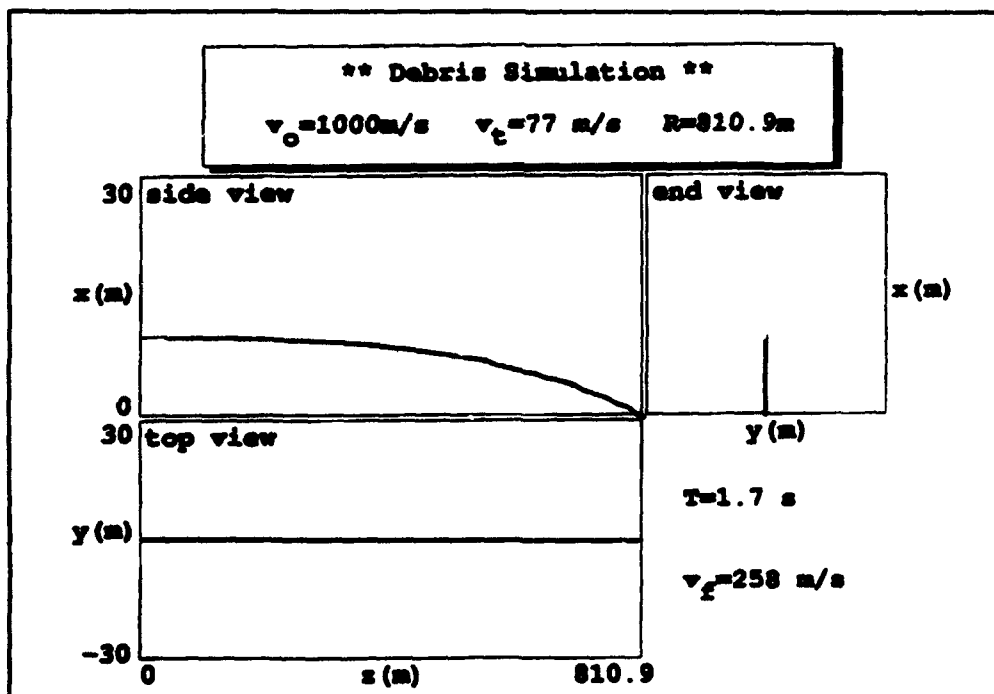


Figure 1-2.   Simulation of a missile fragment from 800 meters tracked to a waterline impact.

meters allows a fragment to reach the ship at the waterline with a kinetic energy of $10^5$ joules breaching hull integrity. This range of 800 meters we call the "critical range". If we return now to Figure 1-1 and compare with this critical range, we find the best case scenario provides a 5% probability of hitting the threat and therefore a 0% probability of a kill prior to it achieving a range that will inflict damage on the ship. If we use 20 fragments and randomize their size, trajectory and velocity, we find in Figure 1-3 that at the critical range of 800 meters 60% of
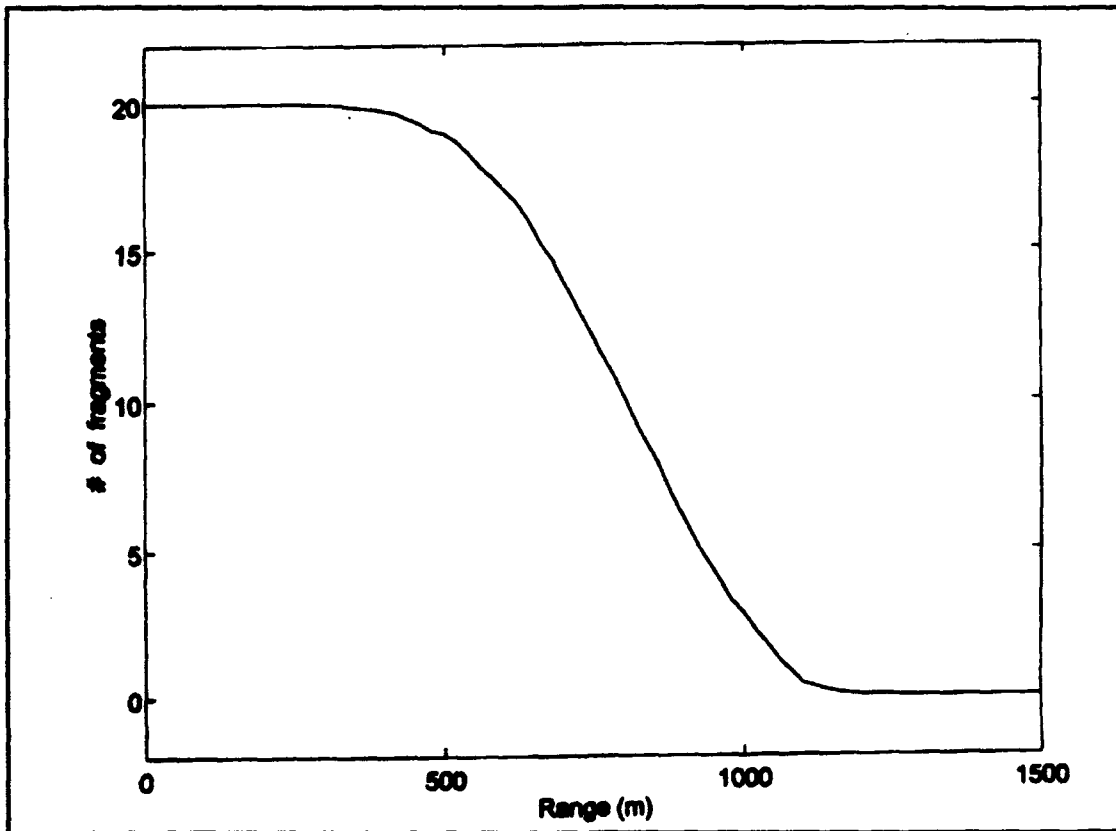


Figure 1-3. Results of tracking 20 missile fragments through various ranges to impact.

4

the fragments reach the ship. Inside of 500 meters 100% of the fragments hit the ship. So, what is the answer for close-in point defense where offensive missiles have been maximized to defeat conventional defensive systems? Speed of light weapons which can reach farther than the 2 km limit of the phalanx.

## B.    LASER CLOSE-IN WEAPONS SYSTEM

In order to destroy an incoming missile, the laser power required on the missile surface is about 2 kW/cm$^2$ over a 5 cm radius spot for a one second duration. The power required at the missile is then 160 kW. Due to the aerosols at sea level, the power from the ship to the target diminishes exponentially by, $P = P_0 \, e^{-\alpha z}$, where $P_0$ is the power at the source, $\alpha = 5 \times 10^{-2}$ km$^{-1}$ is the extinction coefficient and z is the range from the source to the target. Based on a range of 20 km for this new system, the required power leaving the ship is 427 kW and equates to a beam director radius of 0.5 m. A tunable FEL utilizing a beam energy $\gamma mc^2 = 50$ MeV and peak current $\hat{I} = 300$ A can have sufficient average current to provide 374 kW at the target. This is more than double that required to kill the missile. An advantage of a speed of light weapon is the fact that based on the missile velocity of $v_0 = 1000$ m/s the laser beam takes t = $6.67 \times 10^{-5}$ s to reach the target. In that amount of time the missile only travels 6.7 cm. Even if the missile is maneuvering, it will not out-maneuver a speed-of-light weapon. The

5

parameters required to achieve this peak power are achievable, and have been demonstrated in existing FELs. But, high average power has not been demonstrated. The speed-of-light weapon has the advantage of killing a missile early enough to allow a greater numbers of engagements. It also allows the operator to assess his success in defeating the missile in seconds allowing the tactician to move on to the next threat.

Why use an FEL instead of current proven conventional lasers? Conventional lasers of the required power utilize gases which are both highly corrosive and deadly Further, with each firing of the weapon you deplete your resources, and therefore have a limited magazine. The FEL requires no gases and as long as there is power to the ship your magazine is never empty. In a typical war-at-sea scenario, the enemy is required to overwhelm the defender with large numbers of threats to assure a 100% probability of destruction of his target. Against a speed-of-light defense coupled with current technology long range anti-missile missiles, the number of offensive missiles to assure a kill becomes prohibitive.

# II. FREE ELECTRON LASER THEORY

## A. GENERAL

Typical lasers essentially take some form of energy to excite a lasing medium. During the decay from these excited states, light is radiated amplifying light of the same wavelength, phase and propagating in the same direction as the stimulating energy. From the initial energy, a coherent, monochromatic light is produced. By contrast, the FEL produces coherent, monochromatic light from the acceleration of relativistic electrons. A magnetic field exerting a force on a relativistic electron bends its trajectory and electromagnetic theory then demands that the electron emit radiation. For a relativistic electron, the power radiated is $P = (2/3)(\gamma^4 e^2 c/R^2)$ [2], where, $e$ is the charge of the particle, $c$ is the velocity of light, $R$ is the bending radius, and $\gamma$ is the energy $E/mc^2$. A relativistic particle when accelerated radiates into a narrow cone pointing in the direction of its motion. If the electrons are subjected to an alternating magnetic field causing them to wiggle or undulate, they will then radiate light along a single axis. As this radiation builds up, the electrons radiate in the presence of radiation. Figure 2-1 illustrates the dynamics by which the electron beam energy is converted into coherent radiation. A single electron traversing one period of an undulator is followed while studying its interaction with the light wave. In frame (a) the short

wavelength optical electric field at the electrons' position is a maximum and is oriented in the same direction as the long wavelength undulator deflection. This orientation decelerates the electron and causes it to give energy to the optical field. In frame (b) the electron has traveled one-fourth of an undulator period at a speed less than $c$, allowing the optical wave to advance on the electron by one-fourth of an optical wavelength. Here the optical electrical field and the undulator field are zero. Except for the force of the undulator, the electron feels no additional force. Again in frame (c) the optical electric field decelerates the electron. Finally in frame (d) the electron has traversed a full undulator period while the optical wave has moved a full optical wavelength over the electron. This idealized phase relationship demonstrates the electron and optical interaction at resonance. The more complex case where a beam of electrons and the optical wave are in a large, number of random phase combinations means that while some electrons are decelerated, others are accelerated. A consequence of this complex energy exchange is that the electrons form electron bunches which collectively exchange energy to the radiation field.
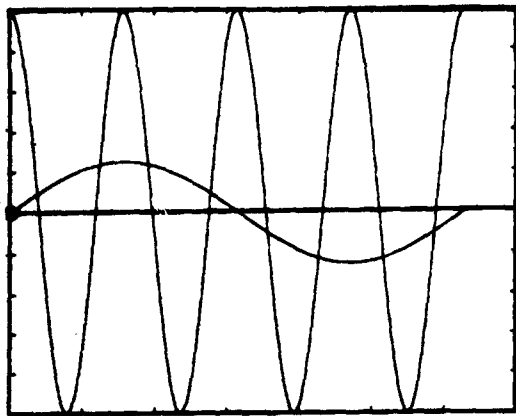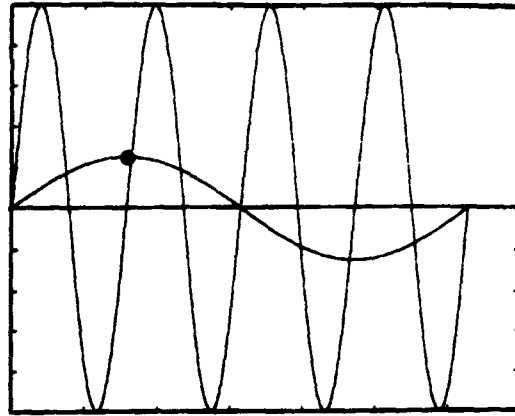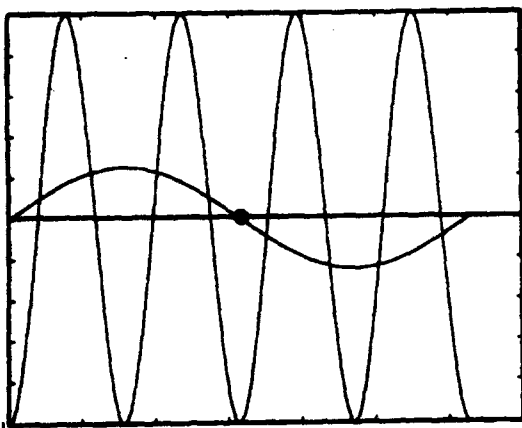
Figure 2-1. Illustration of the electron and optical wave interaction beginning with frame (a) (upper left), advance of the optical wave through a quarter of the undulator period in frame (b) (upper right). Frame (c) (lower left) is halfway through the undulator and finally frame (d) (lower right) is full passage through one period of the undulator.
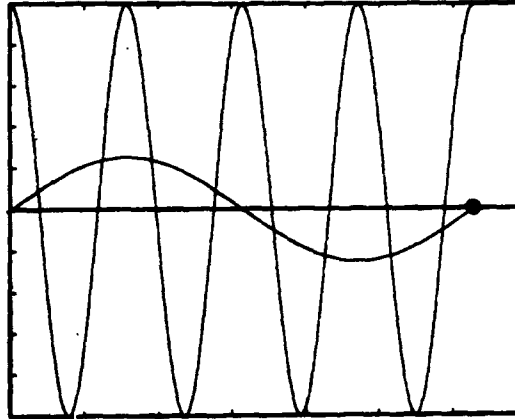
## B.   BASIC PRINCIPLES.

We examine a linearly-polarized undulator producing coherent linearly-polarized light.  The undulator field is described by [3]

$$\bar{B}_u = B \ [0, \ \sin(k_0 z), \ 0] \qquad\qquad 2\text{-}1$$

along the undulator (z) axis where $B$ is the undulator peak magnetic field and $k_0 = 2\pi/\lambda_0$ is the undulator wavenumber.  The undulator length is $L = N\lambda_0$, where $\lambda_0$ is the undulator wavelength and $N$ is the number of undulator periods.  The undulator provides a periodic transverse deflection to the electrons causing them to radiate spontaneously.  As this spontaneous emission grows,  an electron with energy $\gamma(t)mc^2$ couples with the co-propagating radiation and exchanges energy with the optical pulse.  The optical wave has an electric field with strength $E$ and carrier frequency $\omega = kc = 2\pi c/\lambda$ where $k$ is the optical wavenumber, $\lambda$ is the optical wavelength, and $c$ is the speed of light.  The optical  mode created by an electron traveling through the undulator can be described by [3]

$$\bar{E} = E(z,t) \ [\cos \psi, \ 0, \ 0]$$
$$\bar{B} = \hat{z} \times \bar{E} = E(z,t) \ [0, \ \cos \psi, \ 0] \qquad\qquad 2\text{-}2$$

where $E(z,t)$ is the wave amplitude, $\psi = kz - \omega t + \phi(z,t)$, and the optical phase is represented by $\phi(z,t)$.  These fields can be derived from the vector potential

$\bar{A}(x,t) = (E(z,t)/k)$ [sin $\psi$, 0, 0]. If the amplitude $E$ and phase $\phi$ are held constant, then these fields describe a plane wave traveling in the z-direction.

## C. ELECTRON DYNAMICS AND THE PENDULUM EQUATION

The Lorentz force acting on an electron traveling through the undulator is

$$\frac{d(\gamma\bar{\beta})}{dt} = -\frac{e}{mc}\left(\bar{E} + \bar{\beta} \times (\bar{B} + \bar{B}_u)\right), \qquad \text{2-3}$$

$$\frac{d\gamma}{dt} = -\frac{e}{mc}\left(\bar{\beta} \cdot \bar{E}\right), \qquad \text{2-4}$$

$$\gamma^{-2} = 1 - \bar{\beta} \cdot \bar{\beta}, \qquad \text{2-5}$$

where, $\bar{B}_u$ is the undulator magnetic fields described by 2-1, $\bar{E}$ and $\bar{B}$ are the optical electric and magnetic field described by 2-2. Substitution of these fields into 2-3 yields

$$\frac{d(\gamma\bar{\beta})}{dt} = -\frac{e}{mc}\left[E(1 - \beta_z)(\cos\psi, 0, 0) + B\beta_z(-\sin(k_0 z), 0, 0)\right]. \qquad \text{2-6}$$

Assuming the electrons are relativistic, $\beta_z \approx 1$, we then have

$$\frac{d(\gamma\bar{\beta})}{dt} \approx -\frac{e}{mc} B\beta_z(-\sin(k_0 z), 0, 0). \qquad \text{2-7}$$

11

Now integrate to obtain the transverse electron velocity

$$\bar{\beta}_\perp = -\frac{\sqrt{2}K}{\gamma}(\cos{(k_0 z)}, 0, 0) , \qquad \text{2-8}$$

where we have assumed perfect electron injection, so the constant of integration is zero. The undulator parameter $K = eB_{rms}\lambda_0/2\pi mc^2$ is a dimensionless quantity characterizing the properties of the undulator, and $B_{rms}$ is the rms field strength in each period. Substitution into 2-5 and averaging over an undulator period, gives

$$\beta_z^2 = 1 - \frac{1 + K^2}{\gamma^2} . \qquad \text{2-9}$$

Taking the time derivative, we get

$$\beta_z\dot{\beta}_z = \frac{(1+K^2)\dot{\gamma}}{\gamma^3} \implies \dot{\gamma} = \beta_z\dot{\beta}_z\frac{\gamma^3}{1+K^2} . \qquad \text{2-10}$$

Substituting the electric field 2-2 into 2-4 and using the value of $\bar{\beta}_\perp$ in 2-8, we have

$$\frac{d\gamma}{dt} = \frac{eKE}{\sqrt{2}\gamma mc}\cos(\psi + k_0 z) = \frac{eKE}{\sqrt{2}\gamma mc}\cos(\zeta + \phi) \qquad \text{2-11}$$

where the electron phase is $\zeta = (k+k_0)z-\omega t$. For phases such that $-\pi/2 < \zeta+\phi < \pi/2$, the electron gains energy from the radiation field, whereas for phases such that

12

$\pi/2 < \zeta + \phi < 3\pi/2$, the electron gives up energy to the radiation field. If we differentiate the electron phase twice we get $d^2\zeta/dt^2 = c(k+k_0)\, d\beta_z/dt$. Substituting 2-10 into 2-11 yields the electron pendulum equation

$$\frac{d^2\zeta}{dt^2} = \frac{2ek_0KE}{\gamma^2 m} \cos(\zeta + \phi) , \qquad\qquad 2\text{-}12$$

which governs the electron motion in the presence of the undulator and radiated fields. Introducing the dimensionless time $\tau = ct/L$ and averaging the motion over each undulator period [3], we have

$$\frac{d^2\zeta}{d\tau^2} = |a| \cos(\zeta + \phi) , \qquad\qquad 2\text{-}13$$

where the dimensionless optical field strength is given by $|a| = 4\pi NeEK(J_0(\xi) - J_1(\xi))L/\sqrt{2}\,\gamma^2 mc^2$, $J_0$ and $J_1$ are Bessel functions of the first kind and $\xi = K^2/2(1+K^2)$. We further define the dimensionless phase velocity by

$$\nu(\tau) = \frac{d\zeta}{d\tau} = L[(k+k_0)\beta_z - k] . \qquad\qquad 2\text{-}14$$

When $\nu = 0$, the electron experiences resonant undulator and radiation field forces.

13

The resonance condition can then be expressed by $\lambda = \lambda_0(1+K^2)/2\gamma^2$. This equation shows that the desired operational wavelength may be achieved by altering the electron beam energy $\gamma$, the undulator wavelength $\lambda_0$ or the undulator parameter $K$. The values of $\lambda_0$ and $K$ are limited by undulator technology; hence most FELs currently operate in the infrared or visible regime. However, with the large value of $\gamma$ achievable at SLAC, it is possible to achieve much shorter wavelengths, including X rays.

## D.    THE WAVE EQUATION

Using the fields in 2-2 and assuming a slowly-varying amplitude and phase such that the terms with two derivatives may be ignored, we can write the optical wave equation as [3]

$$
\left(\frac{\partial^2}{\partial z^2} - \frac{1}{c^2}\frac{\partial^2}{\partial t^2}\right)\bar{A}(x,t) \approx 2\left[\frac{\partial E}{\partial z} + \frac{1}{c}\frac{\partial E}{\partial t}\right](\cos\psi, 0, 0)
$$

$$
+ 2E\left[\frac{\partial\phi}{\partial z} + \frac{1}{c}\frac{\partial\phi}{\partial t}\right](-\sin\psi, 0, 0) \approx -\frac{4\pi}{c}\bar{J}_\perp .
$$

2-15

The total beam current $\bar{J}_\perp$ is the sum of all single-particle currents, $\bar{J}_{\perp i} = -ec\beta_\perp \delta^3(\bar{x} - \bar{r}_i)$, where the position of the $i$th electron is $\bar{r}_i$ and the transverse motion of the electron is determined 2-8. Separating the wave equation into its fast

14

and slow varying factors and averaging over time gives

$$\left(\frac{\partial}{\partial z} + \frac{1}{c}\frac{\partial}{\partial t}\right) E e^{i\phi} = -\frac{2\sqrt{2}\,\pi e K\,(J_0(\xi)-J_1(\xi))}{\gamma} \sum e^{-i\varsigma}\,\delta^3\,(\bar{x}-\bar{r_i}). \qquad 2\text{-}16$$

The Bessel function factors describe the reduced coupling associated with fast periodic motion in each linearly-polarized undulator period. Following the field envelope traveling at speed $c$, the longitudinal coordinate becomes $z = \bar{z}+ct$, and simplifyies the differential operator from $(\partial/\partial z + c^{-1}\,\partial/\partial t)$ to $c^{-1}\,\partial/\partial t$. With respect to the light, the electrons then drift back with a relative speed $c(1 - \beta_z)$. The summation in the wave equation can be replaced by an average $< e^{-i\varsigma} >$ over sample electrons weighted by the electron particle density $\rho$. This leads to [3]

$$\frac{\partial}{\partial t} E\, e^{i\phi} = -\frac{2\sqrt{2}\,\pi e K\,(J_0(\xi)-J_1(\xi))\,c}{\gamma}\,\rho < e^{-i\varsigma}> . \qquad 2\text{-}17$$

Finally, we introduce the dimensionless time $\tau = ct/L$, and the dimensionless current density $j = 8N(e\pi K(J_0(\xi)-J_1(\xi))L)^2\rho/\gamma^3 mc$, which simplifies the wave equation to

$$\frac{da}{d\tau} = -j\left\langle e^{-i\varsigma}\right\rangle , \qquad 2\text{-}18$$

Where the complex dimensionless field is $a = 4\pi NeK(J_0(\xi)-J_1(\xi))LEe^{i\phi}/\sqrt{2}\,\gamma^2 mc^2$ and

15

is consistent with the definition of the dimensionless field strength found below 2-13.

By assuming a plane wave, this derivation ignores the transverse evolution of the fields. When these effects are included, the three dimensional wave equation can be developed similar to the previous derivation and results in the parabolic wave equation [3]

$$\left(-\frac{i}{4}\bar{\nabla}_{\perp}^{2} + \frac{\partial}{\partial \tau}\right) a(\bar{x}, \bar{y}, \bar{z}, \tau) = -\left\langle j\, e^{-\kappa}\right\rangle.$$ 
2-19

Here, $\nabla_{\perp}^{2} = \partial_{x}^{2} + \partial_{y}^{2}$ and defines the transverse diffraction of the optical wave. The growth of the optical wave in the longitudinal direction is described by 2-19.

## E. ELECTRON BEAM QUALITY

Of some concern to the FEL is the quality of the beam which feeds the undulator and determines its interaction with the light. One measure of the quality of the beam is the emittance. The emittance, $\varepsilon$, is the average angular spread times the average beam radius, and the normalized emittance is $\varepsilon_{n} = \varepsilon \gamma$. The effect of electron beam emittance is to produce an effective velocity spread in the z direction which disturbs the FEL resonance condition [4]. As a minimum condition the transverse cross-section of the electron beam must be smaller than

that of the photon beam [5]. When we equate these conditions we arrive at

$$\varepsilon \leq \frac{\lambda}{4\pi},$$ 2-20

where $\lambda$ is the shortest wavelength for which spatial coherence is desired [6]. Substitution of $\lambda$= 4 nm shows a required normalized emittance less than $\varepsilon_n$=3.2 mm-mrad. This is within the realm of current technology. If we project to the programs logical conclusion, achievement of hard X rays in the 0.15 nm regime, the required beam quality will be $\varepsilon_n$ =1 mm-mrad.

# III. SLAC X RAY FREE ELECTRON LASER

## A. SLAC PROPOSAL

Live cell holography and high resolution imaging of DNA base pairs are two potential biological applications of an X ray laser [7]. The 2 to 4 nm wavelength arena corresponds to the "water window" where water becomes transparent to soft X rays. The duration of the pulse can be short enough that a biological sample will be unaffected by the radiation.

The Free Electron Laser (FEL) appears to be the best possible source for an X ray laser. An advantage is that the FEL requires no light source and produces coherent radiation from noise in a process called Self Amplified Spontaneous Emission (SASE). Through this mechanism coherent X rays are created in a single pass which obviates the requirement for an X ray light source to feed the laser and
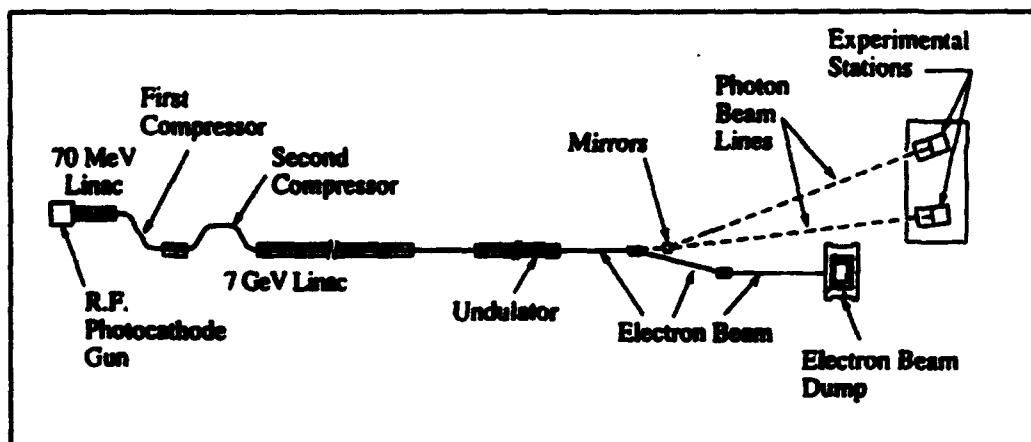


Figure 3-1. Schematic of the Slac linac driving a coherent X ray FEL.

the need for mirrors. Figure 3-1 is a schematic of the proposed system combining

the SLAC linac with an undulator to produce coherent X rays. The system design

would incorporate part of the SLAC linac to accelerate the electron beam to an

energy of $\gamma mc^2$= 7 GeV with a peak current of I=2500 A and a bunch length of

0.16 picoseconds. These pulses are injected into an undulator with a period of $\lambda_0$

= 8 cm and a proposed length of 60 m, producing light of 4 nm wavelength and

a peak power of 28 GW. Using three sections of the linear accelerator separated

by two compression stages the electron bunch is accelerated from 10 MeV to the

desired 7 GeV. Table 3-1 contains the design parameters for the X ray FEL

| ELECTRON BEAM | | UNDULATOR | |
|---|---|---|---|
| Energy     $\gamma mc^2$ | 7 GeV | Undulator Length     L | 6000 cm |
| Peak Current | 2500 A | Period     $\lambda_0$ | 8.3 cm |
| Energy Spread     $\Delta\gamma/\gamma$ | 0.04% | Undulator Parameter     K | 4.2 |
| Normalized Emittance     $\varepsilon_n$ | 3.0 mm-mrad | LASER PROPERTIES | |
| Pulse Length | 0.16 ps | Wavelength     $\lambda$ | 4 nm |
| Beam Radius | 0.0065 cm | Peak Power | 28 GW |

Table 3-1. Proposed parameters for an X ray FEL at SLAC

planned at SLAC[1]. The peak current of 2500 A corresponds to a dimensionless current density $j$ = 4000 and results in the FEL operating in the high gain regime. Most FEL's operate in the low gain regime where $j \sim 1$. The evolution of the electrons through the undulator is governed by the pendulum equation 2-13, while the evolution of the optical amplitude and phase is determined by the optical wave equation 2-18 or 2-19. The dimensionless current determines the response of the optical wave to the electron bunching, coupling 2-13 and 2-18 or 2-19. Utilizing these equations, we initially examine the evolution of the electrons in phase-space ($\zeta$, v). Figure 3-2 is a phase-space plot using the parameters of Table 3-1. At
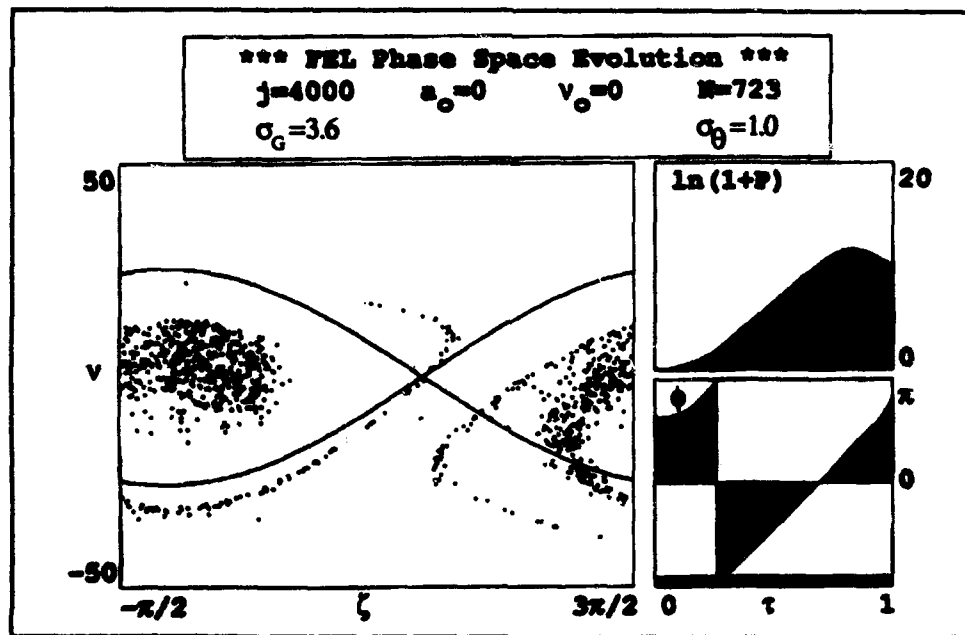


Figure 3-2.   Phase-space simulation where dimensionless current j=4000 (I=2500 A).

startup ($\tau$=0), there is no optical field $a$ = 0. The electrons are all started with random initial phases $\zeta$ between $-\pi/2$ and $3\pi/2$ and periodic boundary conditions are assumed throughout the evolution. The initial electron phase velocities are spread randomly in a Gaussian distribution with standard deviation $\sigma_G$ = 3.6 and average $v_0$ = 0. Superimposed is a random exponential spread with characteristic width $\sigma_\theta$ = 1. The final position of the electrons in the phase-space of Figure 3-2 are bunched in the upper half of the separatrix at the end of the undulator ($\tau$=1). The electrons have overbunched through the undulator and are now taking energy back from the light. The change in phase velocity is related to the change in energy by $\Delta v$ = $4\pi N\Delta\gamma/\gamma$. Ideally, the electrons should be bunched in the lower half of the separatrix, indicating the electrons have given up their energy to the laser light. This is shown in the plot of the logarithmic power evolution from $\tau$=0 to 1 in the upper right hand corner of Figure 3-2. Again we see that the maximum power occurs at approximately $\tau$=¾ and as the electrons begin to overbunch the power diminishes. As the electrons begin to bunch near $\zeta \approx \pi/2$, they drive the optical field phase $\phi$, as shown by the graph in the lower right. This causes the separatrix to shift in phase space, so that the electron bunch is near the optimal relative phase $\zeta+\phi$ = $\pi$ for gain. The simulations show that the laser saturates too early in the undulator and the optical power drops off before it can be utilized. In order to optimize the laser, we can decrease the length of the undulator. Figure 3-3 is a phase space simulation with j=2000 which produces the same results as decreasing

21

the undulator length by about 20%. Now we see that saturation occurs at the end

of the undulator. The electrons are bunched in the lower half of the separatrix at

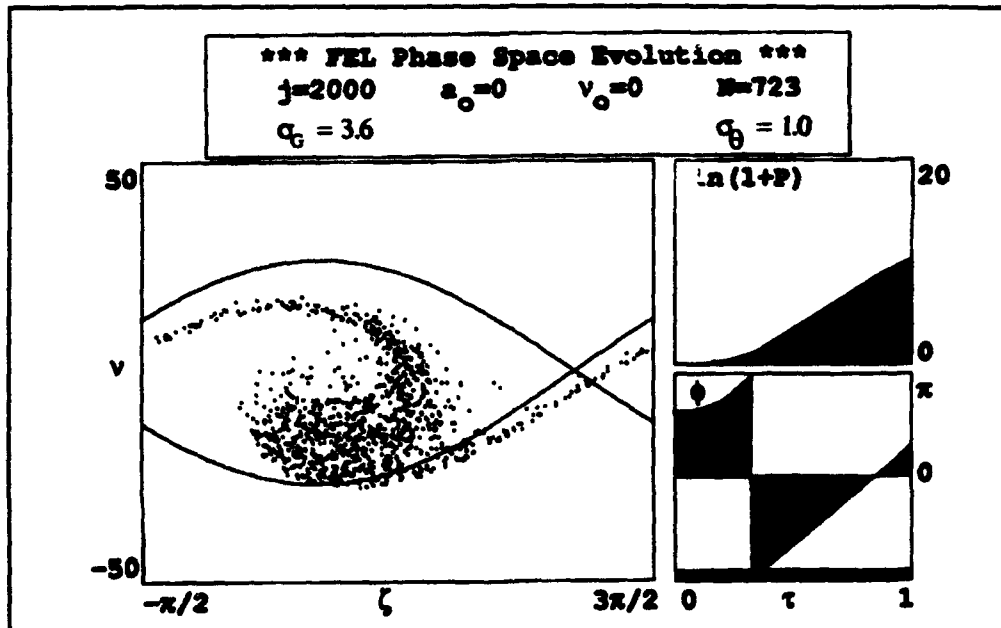the relative phase $\zeta+\phi \approx \pi$ where maximum gain occurs.



Figure 3-3. Phase-space simulation where the dimensionless current j=2000 (I=1250 A).

Another solution to the early saturation and loss in power in the undulator

is to taper the undulator by decreasing the undulator wavelength $\lambda_0$ or decreasing

the field strength $B$. To account for the force due to tapering, the pendulum

equation 2-13 takes the form [3]

$$\frac{d^2\zeta}{d\tau^2} = \delta + |a| \cos(\zeta + \phi) \, ,$$

3-1

where $\delta$ is a constant torque given by $\delta \approx -4\pi N K^2 \Delta B/B(1+K^2)$ if we vary the undulator field strength and by $\delta \approx -2\pi N \Delta\lambda_0/\lambda_0$ if we vary the wavelength. Here, $\Delta B$ and $\Delta\lambda_0$ are incremental changes in the undulator field strength and wavelength respectively. By setting $\zeta = \int_0^\tau k_0(\tau') \, d\tau' + kz - \omega t$ we account for the changing undulator wavenumber $k_0(\tau) = 2\pi/\lambda_0(\tau)$.

In Figure 3-4 the undulator simulated in Figure 3-2 with $j$=4000 is simulated using a taper of $\delta$=50$\pi$. This corresponds to a $\Delta B/B$ = 3% change in the undulator field. Here the acceleration induced by tapering overcomes the natural deceleration of the untapered undulator which would extract optical energy accelerating the electrons. Comparing Figure 3-2 to Figure 3-4 we see that instead of reaching saturation three-fourths of the way through the undulator followed by a drop in power, now we continue to increase power throughout the undulator.
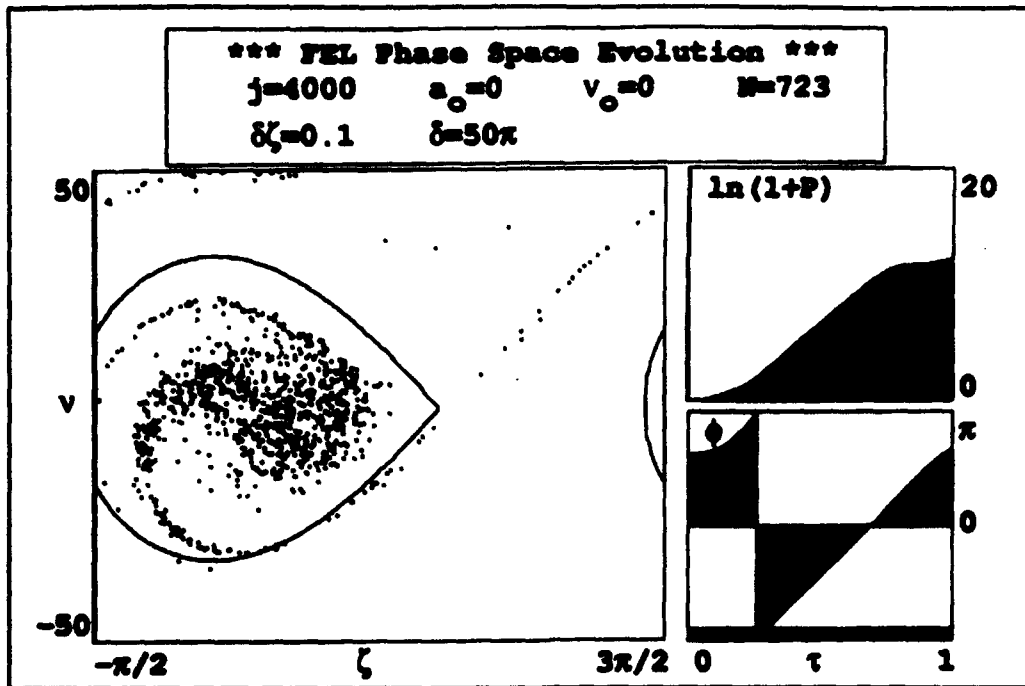
Figure 3-4. Phase-space simulation with a tapered undulator.

## B.    LONGITUDINAL FIELD DEVELOPMENT

The optical field in the longitudinal direction can be generalized by following several sites along the complex wave envelope $a(z)$. We scale our length in the $z$ direction by the slippage distance $N\lambda$, the distance the electron pulse slips back relative to the optical pulse over one pass through the undulator. This corresponds to the distance over which the electrons and light exchange

24

information. The pendulum and wave equations 2-13 and 2-18 can be generalized to [3]

$$\frac{d^2\zeta_{z+\tau}}{d\tau^2} = |a_z| \cos (\zeta_{z+\tau} + \phi_z)$$

3-2

$$\frac{da_z}{d\tau} = -j_{z+\tau} \left\langle \exp (-i\zeta_{z+\tau}) \right\rangle_{z+\tau}.$$

As the electrons at each site pass through the undulator, they interact with a series of optical sites passing information from one site to the next. Figure 3-5 shows the effects of slippage and field growth. In the bottom left we see the exponential gain over the length of the undulator peaking at the end of the undulator. The bottom-middle illustrates the single-mode gain spectrum as a function of frequency around resonance. In the bottom-right window is the power development throughout the length of the undulator. Once light is produced, the power grows exponentially reaching its maximum at the end of the undulator. The middle-left depicts the growth in the amplitude of the light in a window that is two slippage distances in length $-1 < z < 1$. We see starting from noise, significant light develops near $\tau = \frac{3}{4}$ through the undulator corresponding to the previously described power growth in the bottom-right. The middle and top-middle frames show the evolution of the power spectrum. Here we note the triangular tickmark indicates resonance $v = 0$. The rectangular tickmark indicates the wavelength of the final average power and shows development of power at wavelengths which
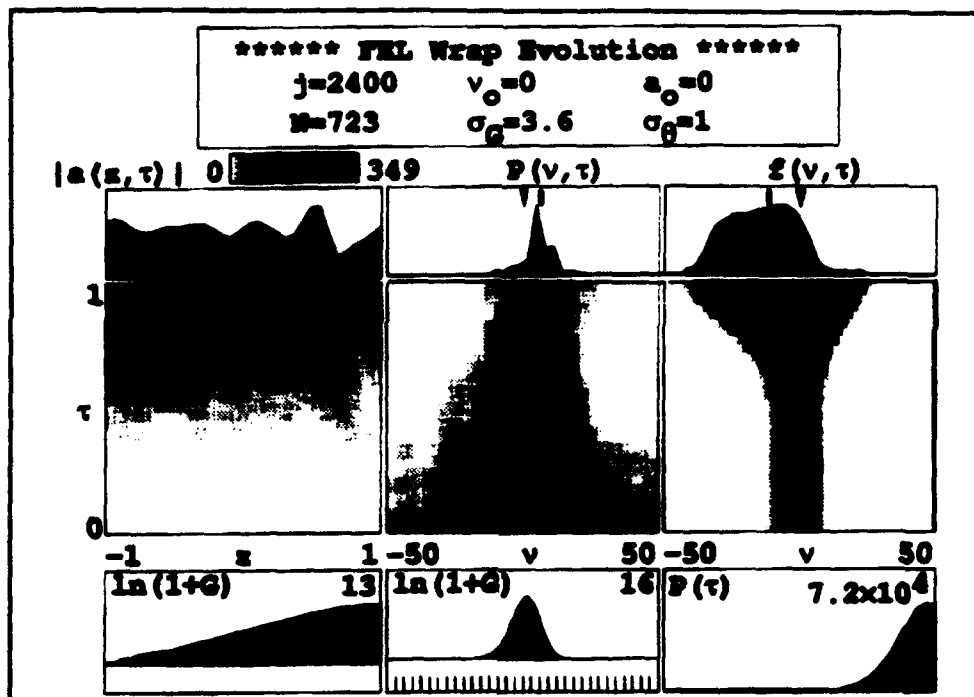
25

Figure 3-5. Coherence evolution simulation showing the effects of slippage.

are higher than the fundamental. Finally, the middle-right and top-right frames show the development of the electron phase velocity distribution. There is a decrease in the average electron phase velocity which corresponds to the development of high optical power. The final phase velocity spectrum (top-right) is spread showing the acceleration of untrapped electrons to larger phase velocities and trapped electrons decreasing in energy. The pointed tickmark indicates the initial electron phase velocity at resonance while the rectangular tick mark indicates

the final average electron phase velocity showing a loss of energy. This shift in

phase velocity accounts for the shift in the power spectrum showing optical power

developing at longer wavelengths than the fundamental.

# IV. THE FUTURE X RAY FEL AND ALTERNATIVES

## A. AFTER THE 4 nm FEL

The 4 nm X ray laser as detailed in Chapter III may be feasible. We now look at the next step into the hard X ray regime. The follow-on experiment at SLAC has wavelength 0.15 nm and is detailed in Table 4-1 [8]. As discussed in Chapter II equation 2-20 the required normalized emittance ($\varepsilon_n$) to achieve full spatial coherence at $\lambda = 0.15$ nm is 1 mm-mrad. Current technology can achieve 3 mm-mrad at 5 GeV. The prognosis is good that RF guns with 1 mm-mrad at 25 GeV will soon be available [8]. Assuming these parameters will be achievable

| ELECTRON BEAM | | UNDULATOR | |
|---|---|---|---|
| Energy $\gamma mc^2$ | 25 GeV | Undulator Length    L | 7000 cm |
| Peak Current | 5000 A | Period    $\lambda_0$ | 4 cm |
| Energy Spread    $\Delta\gamma/\gamma$ | 0.02 % | Undulator Parameter    K | 4.2 |
| Normalized Emittance    $\varepsilon_n$ | 1mm-mrad | LASER PROPERTIES | |
| Pulse Length | 0.16 ps | Wavelength    $\lambda$ | 0.15 nm |
| Beam Radius | 0.0065 cm | Peak Power | 0.17 GW |

Table 4-1. Proposed parameters for 0.15 nm X ray FEL.

we now examine the viability of producing hard X rays in a FEL. Initial simulations show that saturation doesn't occur in the 70 m undulator outlined in Table 4-1. Instead, saturation occurs at 100 m as depicted in Figure 4-1 which is a phase-space simulation of a 150 m undulator. However, saturation yields peak power and for the purposes envisioned for the X ray FEL, power out is not a primary concern. So we need to examine whether coherent light is produced in
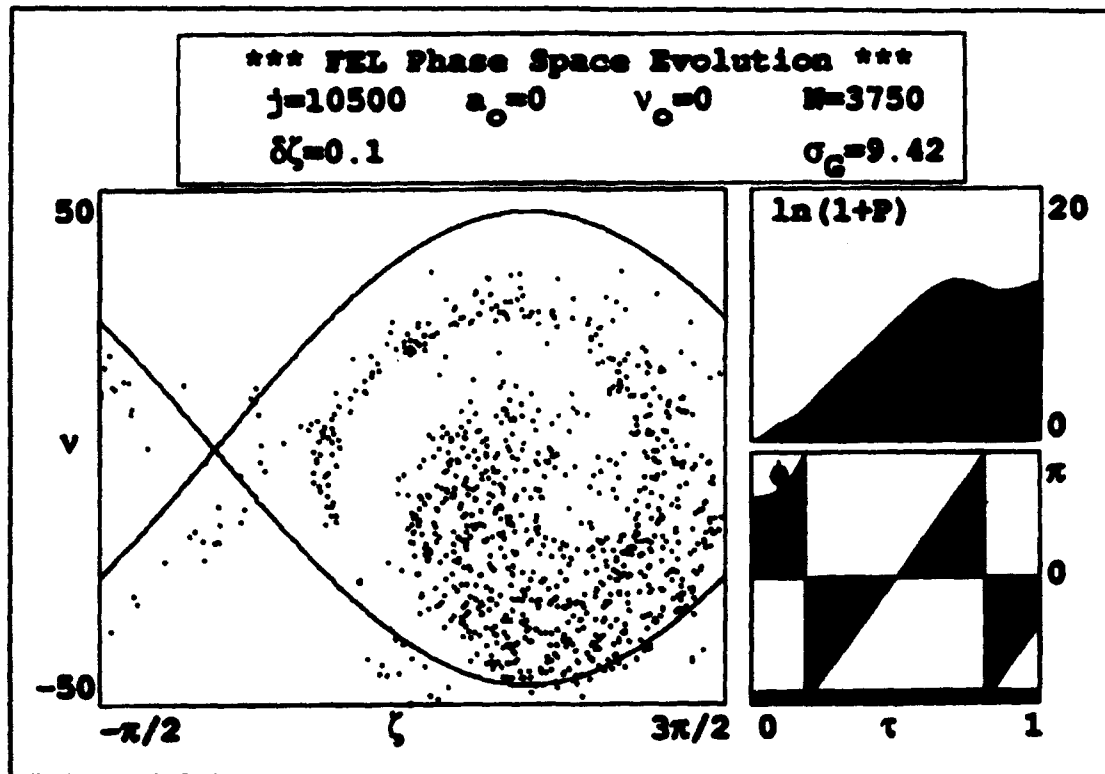


Figure 4-1.  Phase space simulation for 150 m undulator utilizing the parameters outlined in Table 4-1.

a 70 m undulator. Figure 4-2 is a transverse multi-mode simulation examining the effects of optical guiding and mode distortion. Here, we see in the top-left the evolution of light along the length of the undulator and in the top-middle is a cross-section of the light at the end of the undulator. From this simulation we see that in an undulator of 70 m that while we do not achieve saturation we do produce light. The middle row of plots depict the position of the electrons in the beam. The bottom row depicts the average evolution in electron phase velocity which shows that at the end of the undulator the average phase velocity has shifted negatively indicating a loss of energy which has been given up to the production of light. But this simulation does not provide information as to whether the light is coherent along the longitudinal axis.
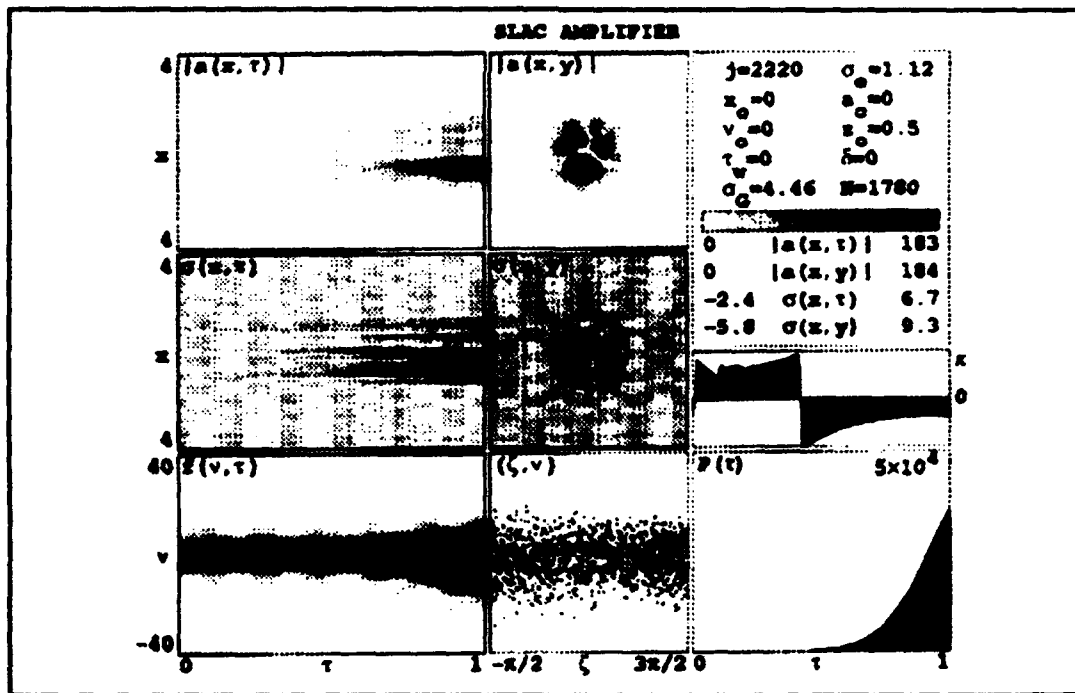


Figure 4-2. Transverse multi-mode simulation examining the effects of optical guiding and mode distortion.

In order to examine the coherence development in this design, again we look at a longitudinal multi-mode simulation in Figure 4-3. We find in the upper left column the development of a window of light through the undulator which is representative of the development of light throughout the undulator. In the middle column we see that light is produced in a narrow bandwidth indicating that the light is indeed coherent. The fractional spread in wavelength is $\Delta\lambda/\lambda \approx \Delta v/2\pi N \approx 9 \times 10^{-4}$. In the bottom right corner is a plot of the dimensionless final power which equates to 170 MW of peak power. These results indicate that upon
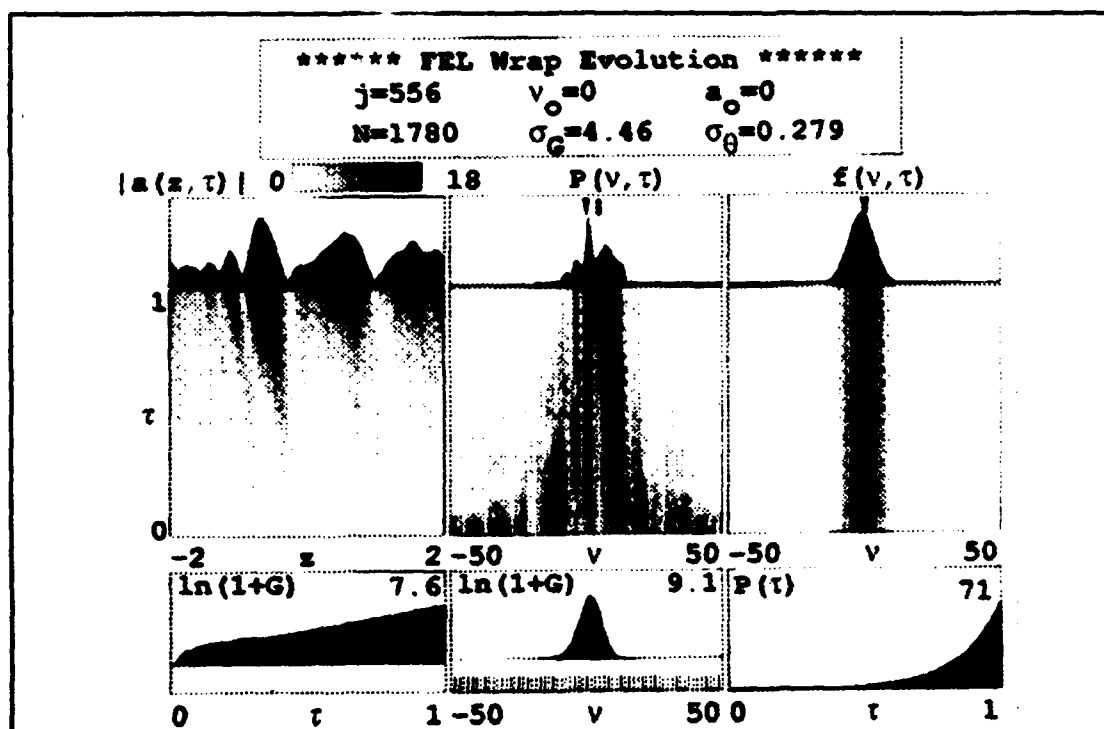


Figure 4-3. Longitudinal multi-mode simulation depicting coherence development.

production of an RF gun which meets the requirements of Table 4-1, the move to hard X rays can be made.

## B.   AN ALTERNATIVE APPROACH.

The design for a 4 nm X ray FEL outlined in Chapter III appears to be viable. However, undulator technology is expensive and the requirement for a 60 m undulator could be quit costly. If the undulator could be shortened and still achieve the same results, that would be a prudent move. An option for boosting the gain in an undulator where we are working with weak optical fields is to add a dispersive section producing a klystron. Here we explore the production of soft X rays with $\lambda$ = 4 nm in a klystron.

| ELECTRON BEAM | | UNDULATOR | |
|---|---|---|---|
| Energy   $\gamma mc^2$ | 5 GeV | Undulator Length    L | 1700 cm |
| Peak Current | 5000 A | Period    $\lambda_0$ | 4 cm |
| Energy Spread        $\Delta\gamma/\gamma$ | 0.02 % | Undulator Parameter    K | 4.2 |
| Normalized Emittance    $\epsilon_n$ | 3 mm-mrad | Dispersive Parameter    D | 0.5 |
| Pulse Length | 0.16 ps | **LASER PROPERTIES** | |
| Beam Radius | 0.0065 cm | Wavelength   $\lambda$ | 0.15 nm |
| | | Peak Power | 2 GW |

Table 4-2.  Proposed parameters for a 4 nm klystron FEL.

In the first undulator section of the klystron, called the "modulator", the electrons are prepared for bunching. While they traverse the dispersive section without interaction with the optical fields, the electrons become bunched. As the enter the second undulator, called the "radiator", the bunched electrons begin to radiate producing coherent light. Table 4-2 lists the parameters for this proposed design. The strength of the dispersive section is described by the dimensionless value $D$ [9]. The effect of the dispersive section is described by $\Delta\zeta = \upsilon D$. The dispersive section strength $D$ was determined by a series of phase space simulations which revealed the most gain was produced with $D = 0.5$. Again to
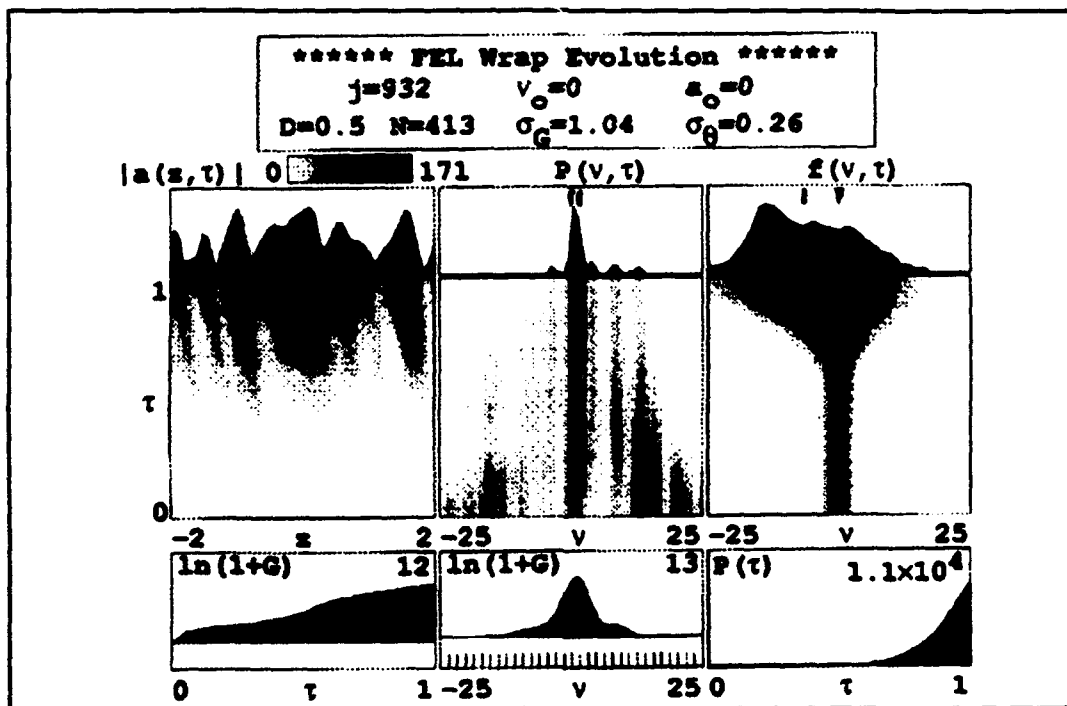


Figure 4-4.   Simulation depicting coherence development for klystron X ray laser.

determine the coherence of the light produced we inspect the results of the longitudinal multi-mode simulation in Figures 4-4 and 4-5. Of primary concern is the middle window in both figures which shows a spike of very narrow bandwidth indicating good coherence development. Both figures are displayed in order to demonstrate that by changing the random number generation in the simulation we randomize the position of the electrons at startup. While the final shape is somewhat altered the development of coherence is still observable. These same variations have been tested with the proposed SLAC X ray laser producing the same coherence results. The right column displays the average electron
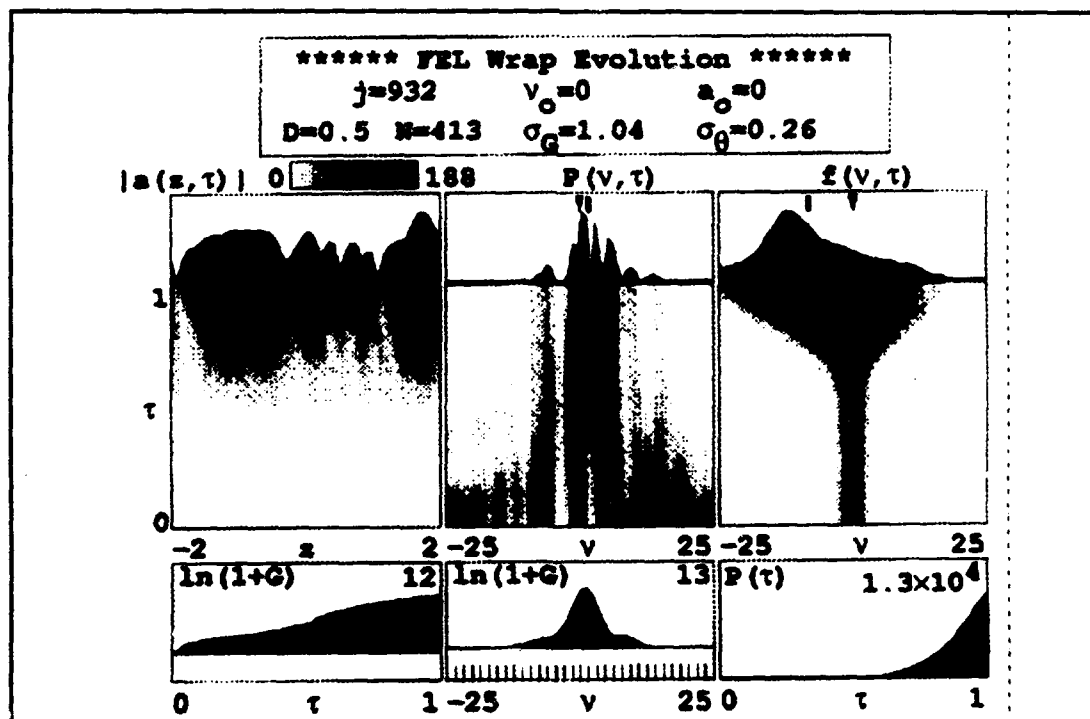


Figure 4-5. Simulation of klystron X ray laser varying electron starting position.

evolution showing maximum loss of energy of the electrons at the end of the radiator. Finally, the power presented in the bottom right equates to 2 GW of peak power. By comparison to the proposed design in Chapter III, we can produce coherent X rays with a 17 m undulator instead of a 60 m undulator which would seem to be advantage in reducing expenses.

# V. CONCLUSIONS

The theory for the FEL which has been presented applies not just to the X ray FEL specifically but to any FEL in general. The tunability which has been shown makes the FEL suitable for many military and industrial applications. The FEL as a shipboard, land based or airborne weapon can respond to a threat at the speed of light and does not require replenishment of a finite magazine. The FEL will have a significant impact upon the military of the future and the defense of the nation.

The proposed X ray FEL is the first viable entry into the regime of coherent X ray light sources. Using the proposed SLAC FEL parameters in Table 3-1, simulation results indicate that X rays in the 4 nm regime are achievable now. The future regime of $\lambda = 0.15$ nm requires an electron beam energy of 25 GeV, a peak current of 5000 A, and $\lambda_0 = 4$ cm which are achievable. However, the required beam quality of $\varepsilon_n = 1$ mm-mrad is not available, but is expected in the near future. This opens the door into a new exciting biological arena for the Free Electron Laser. In Table 5-1, we compare our results with data generated in a coherence and linewidth study by Lawrence Berkeley Laboratory and Lawrence Livermore National Laboratories [10]. The number of undulator periods necessary to reach saturation, $N_{sat}$, is plotted as a function of the dimensionless current density $j$. In this study, LBL and LLNL used the GINGER particle simulation code to evaluate

the effect of current on the FEL. We see that the simulations we report are consistent with their findings.
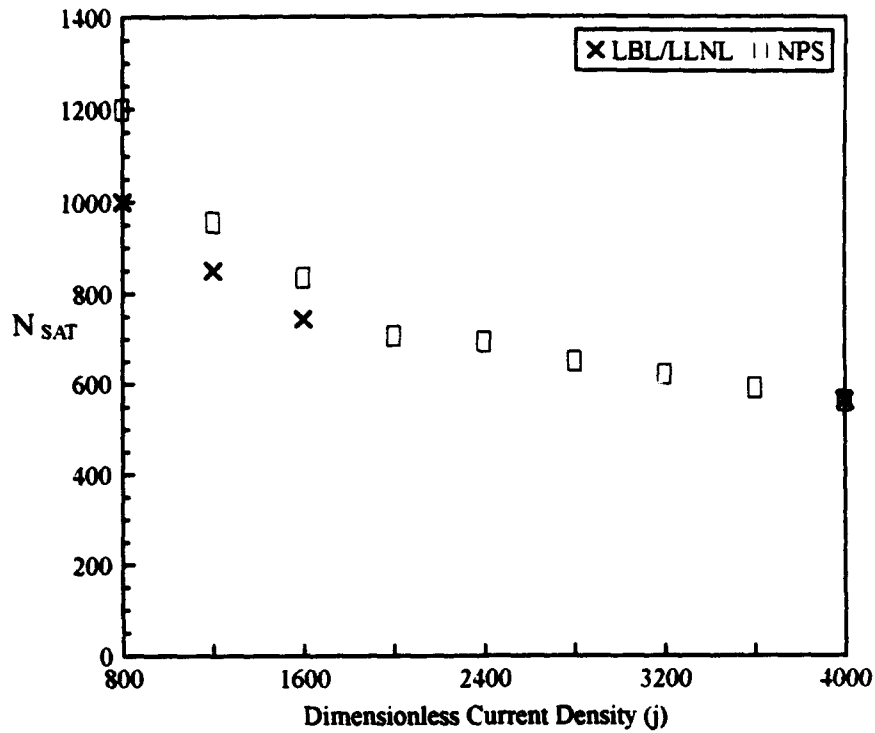


Table 5-1. Data comparison of LBL/LLNL and NPS simulations.

Finally, as an alternative to the currently proposed SLAC X ray laser utilizing a 60 m undulator, we have presented a variation utilizing a klystron. By doing so, the required undulator length is reduced to only 17 m. We have presented simulation results which makes this a feasible and potential cost savings option which requires further investigation.

# LIST OF REFERENCES

[1]    C. Pellegrini, et al., "A 2 to 4 nm Power FEL on the SLAC LINAC", Nuclear Instruments and Methods, A331, pp. 223-227,1993.

[2]    A. M. Sessler and D. Vaughan, "Free-Electron Lasers," American Scientist, Volume 75, pp. 34-43, January - February 1987.

[3]    W. B. Colson, "Classical Free Electron Laser Theory," Laser Handbook, W. B. Colson, C. Pellegrini and A. Reneiri, Volume 6, North-Holland, Amsterdam, 1990.

[4]    E. Haselhoff, Aspects of a Free Electron Laser, pp. 58-65, CIP Gegevens Koninklijke Bibliotheek, Den Haag, 1993.

[5]    A. Steenbergen, "Accelerators and Storage Rings for Free Electron Lasers," Laser Handbook, Colson, W. B., C. Pellegrini and A. Reneiri, Volume 6, pp. 124-134, North-Holland, Amsterdam, 1990.

[6]    D. Atwood, K. Halbach, Kwang-Je Kim, "Tunable Coherent X rays," Science, Volume 228, Number 4705, pp. 1265-1272, 1985.

[7]    "Workshop on Scientific Applications of Short Wavelength Coherent Light Sources," SLAC-414, SLAC/SSRL-0007, CONF-9210278, 1993.

[8]    C. Pellegrini and H. Winick, "A Linac Coherent Light Source," Workshop on Scientific Applications of Coherent X-rays, SLAC-437, SLAC/SSRL-0066, February 1994.

[9]    W. B. Colson and I. Boscolo, "Self-consistent gain in the optical-klystron free-electron laser," Physical Review, Volume 31, Number 4, pp 2353 - 2361, April 1985.

[10]   W. M. Fawley, A.M. Sessler and E.T. Scharlemann, "Coherence and Linewidth Studies of a 4 nm High Power FEL."

# INITIAL DISTRIBUTION LIST

1.  efense Technical Information Center                                      2
    Cameron Station
    Alexandria, Virginia  22304-6145

2.  Library, Code 52                                                         2
    Naval Postgraduate School
    Monterey, California  93943-5002

3.  Professor William B. Colson, Code PH/Cw                                  8
    Department of Physics
    Naval Postgraduate School
    Monterey, California  93943-5002

4.  Professor Robert L. Armstead, Code PH/Ar                                 1
    Department of Physics
    Naval Postgraduate School
    Monterey, California  93943-5002

5.  Professor Claudio Pelligrini                                             1
    Department of Physics
    UCLA
    Los Angeles, California  90024-1547

6.  Professor Herman Winick                                                  1
    SSRL
    PO Box 4349 MS 69
    Stanford, California  94309